PCCP

Cite this: *Phys. Chem. Chem. Phys.*, 2012, **14**, 14999–15002

www.rsc.org/pccp

COMMUNICATION

Air-stable and efficient inorganic–organic heterojunction solar cells using PbS colloidal quantum dots co-capped by 1-dodecanethiol and oleic acid

Sungwoo Kim,†[ab] Sang Hyuk Im,†[a] Meejae Kang,[b] Jin Hyuck Heo,[a] Sang Il Seok,*[a] Sang-Wook Kim,*[b] Iván Mora-Seró*[c] and Juan Bisquert[c]

Received 13th September 2012, Accepted 13th September 2012
DOI: 10.1039/c2cp43223d

PbS colloidal quantum dot (CQD)-sensitized inorganic–organic heterojunction solar cells fabricated by using the PbS CQDs co-capped by the oleic acid (OA) and 1-dodecanethiol (DT) ligand showed better device stability with aging time under ambient conditions without encapsulation. Furthermore, the device performance is better than the cell fabricated from PbS CQDs without DT ligand. The enhancement of performance in OA and DT co-capped systems is investigated by impedance spectroscopy. An upward displacement of the TiO_2 conduction band, with a consequent increase of V_{oc}, results in the improved performance when CQD with DT are employed.

Recently, solar energy conversion devices have been of great interest because solar energy is green, renewable, and sustainable. In particular, since Grätzel *et al.* reported the development of highly efficient dye-sensitized solar cells (D-SSCs),[1] SSCs have been extensively studied to replace conventional solar cells because they are transparent and cost-effective. However, the weak absorption of conventional Ru dyes requires a thick mesoscopic TiO_2 electrode of $\sim$10 μm, and the liquid redox electrolyte has the potential to leak. These issues seem to pose a problem in finding further applications for conventional D-SSCs, such as flexible solar cells, because bending can cause the thick TiO_2 electrode to break and the liquid electrolyte to leak. Therefore, it is desirable to use a new sensitizer with a strong absorption coefficient and a solid hole transporting material instead of a liquid electrolyte. From this viewpoint, it is beneficial to develop efficient solid-state inorganic semiconductor- or quantum dot-sensitized solar cells (QD-SSCs) because they have a higher absorption coefficient than conventional Ru/organic dyes, convenient bandgap tunability by size control, easier charge separation because of a large intrinsic dipole moment, and multiple exciton generation.[2] Unlike p–n heterojunction solar cells, sensitized solar cells are constructed using three key components: an electron conductor, a sensitizer, and a hole conductor. This unique feature enables SSCs to attain a high energy conversion efficiency because the electron–hole pairs generated in the sensitizer are quickly separated into the electron conductor and hole conductor, which suppresses the recombination of the generated charge carriers. Accordingly, SSCs based on a metal chalcogenide such as CdS(e),[3] PbS,[4] or Sb_2S_3[5] have been intensively studied.

Among the metal chalcogenides, PbS colloidal quantum dots (CQDs) have attracted great attention because their bandgap to a large extent can be controlled by the quantum confinement effect as a result of their narrow bulk energy bandgap (0.41 eV) and small exciton Bohr radius (18 nm).[6] Sargent *et al.*[7] developed efficient PbS CQD Schottky and n–p heterojunction solar cells. We have also fabricated PbS CQD-sensitized solar cells.[4] The main factors for the successful demonstration of efficient solar cells are an optimized device architecture and improved interfacial contact between the PbS CQDs. Device optimization has been used to extend the interfacial area of the n-type electron conductor and p-type PbS CQDs in order to improve the charge transport. However, the performance of PbS CQD-based solar cells tends to quickly degrade upon exposure to air because of the oxidation of the PbS CQDs. Therefore, it is equally important to improve device stability in order to aid commercial application. Very recently, atomic passivation of PbS CQDs[7a] and introduction of a LiF interlayer[7b] between PbS CQDs and counter metal electrode have been proposed to improve the air stability of operating devices. In an effort to improve the air stability of PbS CQDs, in this study we used dodecanethiol as an organic passivator during the colloidal synthesis of PbS CQDs and applied them to PbS CQD-SSCs to improve device stability.‡

Fig. 1(a) and (b) show transmission electron microscopy (TEM) images of the synthesized PbS-OA and PbS-OA-DT CQDs. These images indicate that the average sizes of both CQDs are almost the same (4.5 nm). Therefore, their absorption peaks are located at the same wavelength, $\sim$1150 nm. The slight difference in the apparent morphologies can be attributed to the strong selective bonding of DT molecules onto the {111} faces of PbS nanocrystals, which alters the shape of the growing PbS nanocrystals.[8] The FT-IR spectra of the PbS-OA and PbS-OA-DT CQDs are shown in Fig. 1(c). The symmetric

[a] *Division of Advanced Materials, Korea Research Institute of Chemical Technology, 141 Gajeong-Ro, Yuseong-Gu, Daejeon 305-600, Korea. E-mail: seoksi@krict.re.kr; Fax: +82-42-861-4251; Tel: +82-42-860-7314*
[b] *Department of Molecular Science and Technology, Ajou University, Suwon, 443-749, Korea. E-mail: swkim@ajou.ac.kr; Fax: +82-31-219-2394*
[c] *Photovoltaic and Optoelectronic Devices Group, Departament de Física, Universitat Jaume I, 12071 Castelló, Spain. E-mail: sero@fca.uji.es*
† These authors equally contributed to this work.

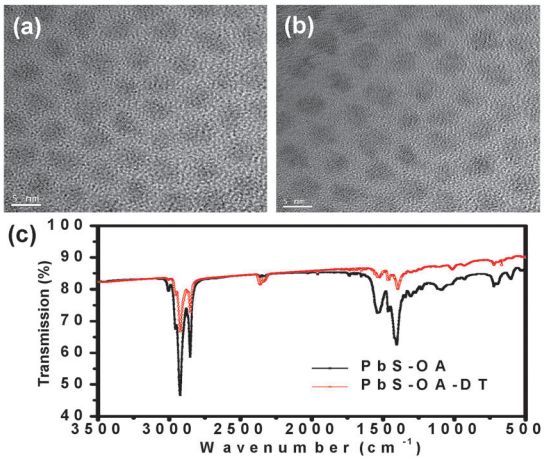

Fig. 1 TEM images of synthesized (a) PbS-OA and (b) PbS-OA-DT CQDs; and (c) their FT-IR spectra.

and antisymmetric C–H stretching vibrations and ═C–H stretching vibration at 2850, 2920, and 3006 cm^{-1}, respectively, indicate the presence of OA on the PbS CQDs.[9] The disappearance of the C═O stretching vibration at 1710 cm^{-1} in OA and the new peak for Pb-oleate at 1544 cm^{-1} confirm the formation of a chemical bond between PbS and OA.[9] The C–S vibration of DT at 1384 cm^{-1} indicates the co-capping of DT molecules on the PbS CQDs, and the missing S–H stretching peak for DT at 2567 cm^{-1} implies the formation of a chemical bond between PbS and DT.[9]

To determine whether the strong bond of DT molecules with PbS CQDs can improve the air stability of the device, we stored the PbS-OA and PbS-OA-DT CQDs in chloroform solutions at room temperature (R) and 120 °C in a convection oven (H), respectively, for 6 h. When the PbS CQD solutions were placed in the convection oven at 120 °C, the chloroform solvent quickly evaporated, and the PbS CQDs were exposed to air for a certain time period. As shown in Fig. 2(a) and (b), the visible–near-infrared (vis-NIR) absorption spectrum of the PbS-OA-A CQDs annealed at 120 °C for 6 h is different from that of the PbS-OA-R CQDs. The blue shift observed in the absorption spectrum during the heat stability test indicates the oxidation of the PbS-OA CQDs. On the other hand, the PbS-OA-DT CQDs did not reveal any change in the absorption spectrum after the stability test. To understand what happened during the stability test, we compared the X-ray photoelectron spectroscopy (XPS) spectra, as shown in Fig. 2(c) and (d). From the S 2p and Pb 4f high-resolution XPS peak analyses,[7c] we can see that the PbS-OA CODs were more severely oxidized to $PbSO_4$ or $PbSO_3$ during the aging test while the PbS-OA-DT CQDs were only slightly degraded. Here, it should be noted that the co-capped DT molecules provided air stability even for relatively large PbS CQDs, whereas only the small PbS-OA CQDs showed air stability because the relatively large PbS-OA CQDs had unpassivated S atoms exposed on the surface of the PbS CQDs, which were likely to be oxidized during the aging test.[7c] The improvement in the air stability of the PbS CQDs by the co-capped DT molecules might be attributed to the fact that the PbS-OA-DT CQDs have some S atoms passivated by the long alkyl chain of DT on the surface, whereas the PbS-OA CQDs had unpassivated

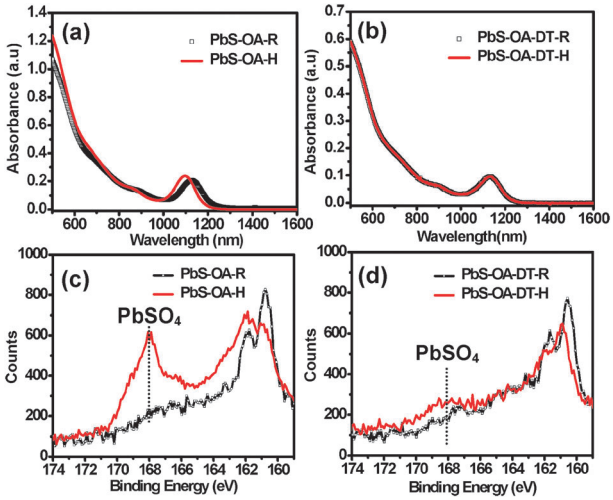

Fig. 2 Visible-NIR absorption spectra of PbS-OA (a) and PbS-OA-DT (b) CQDs with and without accelerated aging at 120 °C for 6 h in a convection oven; and high resolution XPS S 2p spectra of PbS-OA (c) and PbS-OA-DT (d) (R = room temperature, H = aged at 120 °C for 6 h).

S atoms, and the DT molecules act as electron donors preventing the oxidation. The improvement in the air stability of the PbS CQDs by simply using co-capped DT molecules enables us to exploit light with longer wavelength more stably in the fabrication of photovoltaic devices.

On the basis of the fact that co-capped DT molecules can improve the air stability of PbS CQDs, we fabricated PbS CQD-SSCs[4b] to determine whether the PbS-OA-DT CQDs can also improve the device stability. Fig. 3 shows a schematic of the device and its band energy diagram. Under the illumination of light, the PbS CQD sensitizer absorbs the light and generates electron–hole pairs. The generated electrons (holes) are then transferred into the TiO_2 electron conductor (P3HT hole conductor). Typically, PbS CQDs-SSCs are fabricated by multiple spin-casting of a PbS CQD solution on an mp-TiO_2 film using EDT linker molecules and by post-EDT treatment to improve the interfacial contact between PbS CQDs.[4b] The representative EQE spectrum and photocurrent density–voltage (J–V) curve of the PbS-OA-DT CQD-SSC are shown in Fig. 4.

The EQE spectrum indicates that the light (from the visible to NIR region) absorbed by the PbS CQDs is efficiently converted into electricity by this SSC, and the EQE value at 1150 nm reaches ~20%. This implies that this PbS CQD-SSC can be used to detect light in the NIR region. The PbS-OA-DT

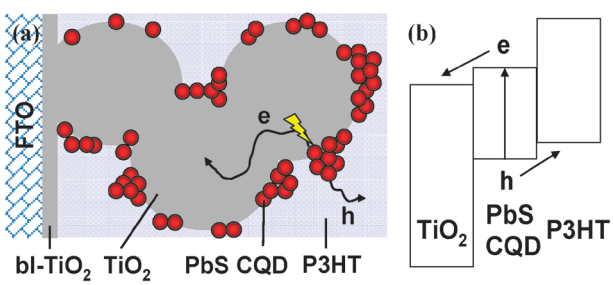

Fig. 3 (a) Schematic of PbS CQD-SSC and (b) its energy band diagram.

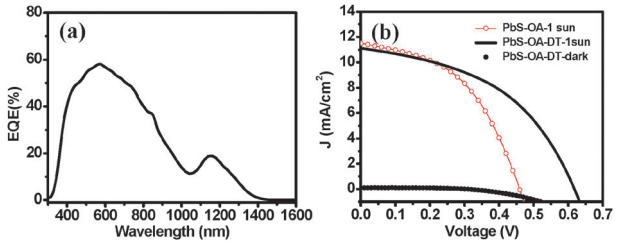

Fig. 4 (a) EQE spectrum and (b) *J–V* curve of PbS-OA-DT CQD-SSC.

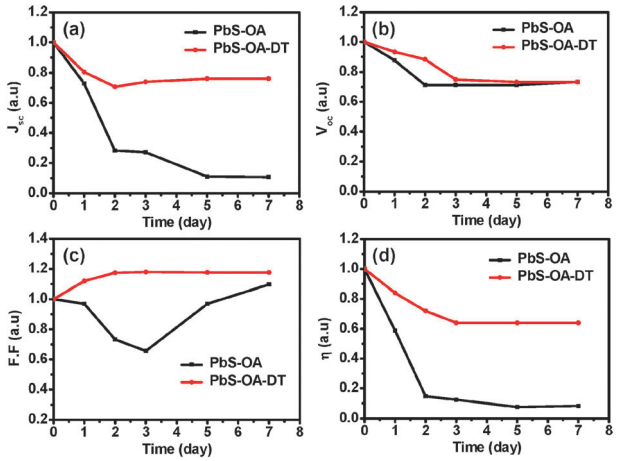

Fig. 5 Air stability of PbS CQD-SSCs with aging time under ambient conditions. (a) Short circuit current density (J_{sc}), (b) open circuit voltage (V_{oc}), (c) fill factor (FF), and (d) power conversion efficiency (η).

CQD-SSC exhibited a short circuit current density (J_{sc}) of 11 mA cm^{-2}, an open circuit voltage (V_{oc}) of 0.61 V, and a fill factor (FF) of 50.4%. Accordingly, it showed an overall power conversion efficiency (η) of 3.3% at 1 sun (100 mW cm^{-2} AM 1.5 G) illumination.

To compare the air stability of the PbS-OA and PbS-OA-DT CQD-SSCs, we fabricated two devices using the same fabrication procedure and measured their *I–V* characteristics at 1 sun illumination. Here, we did not encapsulate the devices but stored them under ambient conditions. The changes in J_{sc}, V_{oc}, FF, and η of the PbS-OA and PbS-OA-DT CQD-SSCs with time are shown in Fig. 5. The initial performance of each device is summarized in Table 1. This clearly indicates that the co-capped DT molecules on the PbS CQD surface can also improve the air stability of an SSC. The improved air stability of the PbS CQD-SSC was resulted in the improved J_{sc} in the cell, because the oxidation layer on the PbS CQDs hinders the charge transfer/transport between PbS CQDs. A degradation of

Table 1 Summary of initial device performances of PbS-OA and PbS-OA-DT CQD-SSCs

	J_{sc}/mA cm^{-2}	V_{oc}/V	FF (%)	η^a (%)
PbS-OA	11.5	0.46	47.2	2.5
PbS-OA-DT	11.0	0.61	50.4	3.3

[a] Unencapsulated devices were measured under 1 sun condition in an air atmosphere.

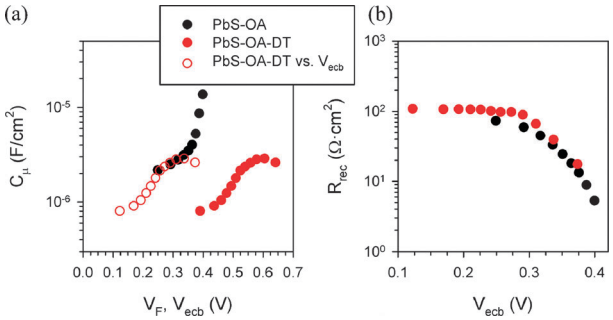

Fig. 6 (a) Chemical capacitance (C_μ), and (b) recombination resistance (R_{rec}) obtained from impedance analysis under 1 sun illumination.

ca. 30% in the power conversion efficiency of the PbS-OA-DT CQD-SSC might be associated with the intrinsically uncapped S atoms, because DT molecules will be bound to the Pb atoms on the surface of the PbS CQDs. The EDT treatment may also cause the PbS CQDs to be oxidized by air because the short EDT linker molecules can quickly replace the longer OA capping ligand and, thus, may reduce the air stability.

To further confirm the role of DT co-capped in PbS CQDs, we compared the impedance spectroscopy (IS) measurements of each device under the working conditions at 1 sun illumination in applying a bias voltage, V_{app}, of 100–700 mV, as shown in Fig. 6. A Nyquist plot of the analyzed samples presents two semicircles assigned, the one at higher frequency, to transport along hole conducting media, and to the charge transfer at the TiO_2/PbS/P3HT interface, at lower frequencies.[10] From the second semicircle, it is possible to obtain the chemical capacitance (C_μ) of TiO_2, Fig. 6(a), and the recombination resistance (R_{rec}) at the interface, Fig. 6(b). Chemical capacitance is represented *vs.* V_F, the voltage drop at the active electrode, simply but subtracting to V_{app} the voltage drop at the series resistance.[11] C_μ shows a significant shift of the chemical capacitance between samples with and without DT, indicating an upward displacement of the TiO_2 conduction band (CB). This displacement can be removed shifting the capacitance and overlapping the capacitances of both samples, Fig. 6(a). In this case the capacitances are represented against a common equivalent conduction band position, V_{ecb}.[11,12] Note that the recombination resistance is dependent on the CB position as it depends on the electron density. R_{rec} does not present any significant change when the CB shift is removed, Fig. 6(b). In this sense, the main effect of DT is an upward shift of TiO_2. This shift enhances the V_{oc} obtained for PbS-OA-DT, see Table 1. Probably DT are working as surface dipoles influencing the TiO_2 CB position as it has been previously reported.[12] Currently, whether DT also affect the position of energy levels in PbS CQDs is under study. Thus DT plays a double beneficial role: (i) shifting up TiO_2 CB, and consequently enhancing the cell V_{oc} and conversion efficiency; and (ii) passivating the CQDs surface increasing the device stability.

In summary, we designed and synthesized PbS CQDs *via* solution chemistry using OA and DT capping molecules to improve the air stability. The PbS CQDs capped by OA and DT molecules (PbS-OA-DT) exhibited much better air stability than the PbS CQDs capped only by OA molecules (PbS-OA) during the accelerated aging test, because the PbS-OA-DT

CQDs had their S atoms passivated by the long alkyl chain of the DT ligand on their surface whereas the PbS-OA CQDs did not have any passivated S atoms on the surface. In addition, PbS-OA-DT coating produces an upward displacement of the TiO_2 conduction band enhancing consequently the V_{oc}. When we applied the PbS-OA-DT CQDs to SSC, we could obtain a power conversion efficiency of 3.3% at 1 sun illumination. The PbS-OA-DT CQD-SSC also exhibited better device stability with aging time under ambient conditions than the PbS-OA CQD-SSC.

Acknowledgements

This work was supported by the Global Research Laboratory (GRL) Program, the Global Frontier R&D Program on Center for Multiscale Energy System, and the Priority Research Centers Program (2009-0093826) funded by the National Research Foundation in Korea, and by a grant from the KRICT 2020 Program for Future Technology of the Korea Research Institute of Chemical Technology (KRICT), Republic of Korea.

Notes and references

‡ Methods:

Synthesis of PbS CQDs: 0.25 mmol of lead(II) acetate trihydrate (Aldrich, 99.999%, 94.375 mg), 0.5 mmol of oleic acid (TCI, 99%, 141 mg), and 0.5 mmol of 1-dodecanethiol (DT: Aldrich, 101 mg) were mixed in a three-necked round bottomed flask (RBF). The mixed solution was degassed by stirring under vacuum at 100 °C for 2 h. After cooling to 60 °C, we added 4 mL of diphenyl ether (Sigma-Aldrich, 99%) and degassed it at 65 °C for 30 min. The temperature was then increased to 155 °C under a N_2 atmosphere, and 0.05 mmol of tri-*n*-octylphosphine (TOP: Stream, 97%) and 0.05 mmol of bis(trimethylsilyl)sulfide (TMS: Acros, 95%) injection solutions were rapidly added to the three-necked RBF at 150 °C. The reaction solution was kept at 120 °C for 30 min and then cooled to room temperature. The synthesized PbS CQDs (PbS-OA-DT) were purified by repeated precipitation for three times using ethanol–isopropanol and re-dispersion in hexane. The reference PbS CQDs without the DT capping ligand (PbS-OA) were synthesized by the same procedure by using 1.25 mmol of OA instead of 0.5 mmol of OA and 0.5 mmol of DT.

Device fabrication: A 1 μm-thick mesoporous TiO_2 (mp-TiO_2: average particle size = 50 nm, crystalline phase = anatase) photoanode film was prepared by screen printing on a dense blocking TiO_2 layer (bl-TiO_2: 50 nm thick)/F-doped SnO_2 (FTO, Pilkington, TEC15) glass substrate[5a] and by subsequent calcination at 500 °C for 1 h in air. The interface of the mp-TiO_2 film was then treated using 20 mM of aqueous $TiCl_4$ solution at room temperature for 12 h and sintered at 450 °C for 15 min. To fabricate PbS CQD-SSCs, 100 μL of the PbS CQDs (PbS-OA-DT) in a hexane–1,2 dichlorobenzene (10/1 vol/vol) solution (15 mg mL^{-1}) was spin-coated on a 3-mercaptopropionic acid (MPA: Aldrich) pre-treated mp-TiO_2 film at 2500 rpm for 20 s. The film was washed with chloroform during spin-coating. In order to multiply stack the PbS CQDs, 250 μL of a 1 wt% EDT (1,2-ethanedithiol)–ethanol solution was spin-coated at 2500 rpm for 20 s, and the PbS CQD solution was then spin-coated at 2500 rpm for 20 s. We repeated spin-coating 15 times for the EDT and PbS CQDs. The P3HT (poly-3-hexylthiophene) solution (Rieke Metals, >98% regioregular: 15 mg mL^{-1} in 1,2-dichlorobenzene) was then spin-coated on the PbS CQD-deposited film at 2500 rpm for 1 min. Poly(3-4-ethylenedioxythiophene) doped with poly(4-stylenesulfonate) (PEDOT:PSS; Baytron AI 4083) solution–methanol (1/2 vol/vol) was spin-coated at 2000 rpm for 30 s, and a 60 nm-thick Au counter electrode was then deposited using thermal evaporation. To improve the interfacial contact between the PbS CQDs, the PbS CQD-SSCs were immersed in a 10 wt% EDT ethanolic solution for 15 h. The EDT post-treated devices were then rinsed with ethanol and dried at 60 °C in an oven for 5 min.

Device characterization: The current–voltage (*I–V*) characteristics of the solar cell were measured using a solar simulator (Class A, 91195A; Newport) with a source meter (Keithley 2420) and a calibrated Si-reference cell (certified by NREL) under 1 sun (100 mW cm^{-2}) illumination. The external quantum efficiency (EQE) was measured using a completely computerized home-designed system comprising a light source (1000 W xenon lamp, Newport, 69935) with a monochromator (Newport cornerstone 260) and a multimeter (Keithley 2002). The active area of the PbS CQD-SSCs for *I–V* characterization was fixed at 0.16 cm^2, and the *I–V* curves were measured by placing a 0.096 cm^2 metal mask on the active area. Impedance measurements were carried out with a GSTAT-30 from Autolab, by applying 100 to 700 mV in a step of 50 mV under light.

1 T. Bessho, S. M. Zakeeruddin, C.-Y. Yeh, E. W.-G. Diau and M. Grätzel, *Angew. Chem.*, 2010, **122**, 6796.
2 A. J. Nozik, *Chem. Phys. Lett.*, 2008, **457**, 3.
3 (*a*) S. H. Im, Y. H. Lee and S. I. Seok, *Electrochim. Acta*, 2010, **55**, 5665; (*b*) Y. H. Lee, S. H. Im, J. H. Rhee, J.-H. Lee and S. I. Seok, *ACS Appl. Mater. Interfaces*, 2010, **2**, 1648; (*c*) Y. H. Lee, S. H. Im, J.-H. Lee and S. I. Seok, *Electrochim. Acta*, 2011, **56**, 2087; (*d*) S. H. Im, Y. H. Lee, S. I. Seok, S. W. Kim and S.-W. Kim, *Langmuir*, 2010, **26**, 18576.
4 (*a*) S. H. Im, J. A. Chang, S. W. Kim, S.-W. Kim and S. I. Seok, *Org. Electron.*, 2010, **11**, 696; (*b*) S. H. Im, H.-j. Kim, S. W. Kim, S.-W. Kim and S. I. Seok, *Energy Environ. Sci.*, 2011, **4**, 4188.
5 (*a*) J. A. Chang, J. H. Rhee, S. H. Im, Y. H. Lee, H.-J. Kim, S. I. Seok, Md. K. Nazeeruddin and M. Grätzel, *Nano Lett.*, 2010, **10**, 2609; (*b*) S. H. Im, C.-S. Lim, J. A. Chang, Y. H. Lee, N. Maiti, H.-j. Kim, M. D. Nazeeruddin, M. Grätzel and S. I. Seok, *Nano Lett.*, 2011, **11**, 4789; (*c*) S. H. Im, H.-j. Kim, J. H. Rhee, C.-S. Lim and S. I. Seok, *Energy Environ. Sci.*, 2011, **4**, 2799; (*d*) C.-S. Lim, S. H. Im, J. H. Rhee, Y. H. Lee, H.-j. Kim, N. Maiti, Y. Kang, J. A. Chang, M. D. Nazeeruddin, M. Grätzel and S. I. Seok, *J. Mater. Chem.*, 2012, **22**, 1107.
6 I. Moreels, K. Lambert, D. Smeets, D. D. Muynck, T. Nollet, J. C. Martins, F. Vanhaecke, A. Vantomme, C. Delerue, G. Allan and Z. Hens, *ACS Nano*, 2009, **3**, 3023.
7 (*a*) J. Tang, X. Wang, L. Brzozowski, D. A. R. Barkhouse, R. Debnath, L. Levina and E. H. Sargent, *Adv. Mater.*, 2010, **22**, 1398; (*b*) J. Tang, L. Brzozowski, D. A. R. Barkhouse, X. Wang, R. Debnath, R. Wolowiec, E. Palmiano, L. Levina, A. G. Pattantyus-Abraham, D. Jamakosmanovic and E. H. Sargent, *ACS Nano*, 2010, **4**, 869; (*c*) X. Wang, G. Koleilat, J. Tang, H. Liu, I. J. Kramer, R. Debnath, L. Brzozowski, D. A. R. Barkhouse, L. Levina, S. Hoogland and E. H. Sargent, *Nat. Photonics*, 2011, **5**, 480; (*d*) J. Tang, K. W. Kemp, S. Hoogland, K. S. Jeong, H. Liu, L. Levina, M. Furukawa, X. Wang, R. Debnath, D. Cha, K. W. Chou, A. Fischer, A. Amassian, J. B. Asbury and E. H. Sargent, *Nat. Mater.*, 2011, **10**, 765.
8 (*a*) J. C. Love, L. A. Estroff, J. K. Kriebel, R. G. Nuzzo and G. M. Whitesides, *Chem. Rev.*, 2005, **105**, 1103; (*b*) M. A. Hines and G. D. Scholes, *Adv. Mater.*, 2003, **15**, 1844.
9 (*a*) D. H. Lee and R. A. Condrate, *J. Mater. Sci.*, 1999, **34**, 139; (*b*) P. Thangadurai, S. Balaji and P. T. Manoharan, *Nanotechnology*, 2008, **19**, 435708; (*c*) S. Chen and W. Liu, *Mater. Chem. Phys.*, 2006, **98**, 183.
10 (*a*) P. P. Boix, G. Larramona, A. Jacob, B. Delatouche, I. Mora-Seró and J. Bisquert, *J. Phys. Chem. C*, 2012, **116**, 1579; (*b*) P. P. Boix, Y. H. Lee, F. Fabregat-Santiago, S. H. Im, I. Mora-Seró, J. Bisquert and S. I. Seok, *ACS Nano*, 2012, **6**, 873.
11 F. Fabregat-Santiago, G. Garcia-Belmonte, I. Mora-Seró and J. Bisquert, *Phys. Chem. Chem. Phys.*, 2011, **13**, 9083.
12 E. M. Barea, M. Shalom, S. Giménez, I. Hod, I. Mora-Seró, A. Zaban and J. Bisquert, *J. Am. Chem. Soc.*, 2010, **132**, 6834.